Applied Radiation and Isotopes 137 (2018) 56–61

Contents lists available at ScienceDirect

Applied Radiation and Isotopes

journal homepage: www.elsevier.com/locate/apradiso

^{64}Cu, a powerful positron emitter for immunoimaging and theranostic: Production via ^{nat}ZnO and ^{nat}ZnO-NPs

Zahra Karimi[a], Mahdi Sadeghi[b,*], Naimeddin Mataji-Kojouri[c]

[a] Department of Medical Radiation Engineering, Science and Research Branch, Islamic Azad University, Tehran, Iran
[b] Medical Physics Department, School of Medicine, Iran University of Medical Science, P.O. Box: 14155-6183, Tehran, Iran
[c] Nuclear Science & Technology Research Institute (NSTRI), Reactor and Nuclear Safety Research School, P.O. Box: 14395-836, Tehran, Iran

HIGHLIGHTS

- ^{64}Cu was produced with zinc oxide nanoparticles (^{nat}ZnONPs) and zinc oxide powder (^{nat}ZnO) via the ^{64}Zn(n,p)^{64}Cu reaction.
- Theoretical and experimental integral yields of ^{64}Cu are calculated.
- The obtained results have been compared with the experimental data.

ARTICLE INFO

Keywords:
ZnONPs
Activity
^{64}Cu
TALYS-1.8
EMPIRE-3.2.2
ALICE/ASH

ABSTRACT

^{64}Cu is one of the most beneficial radionuclide that can be used as a theranostic agent in Positron Emission Tomography (PET) imaging. In this current work, ^{64}Cu was produced with zinc oxide nanoparticles (^{nat}ZnONPs) and zinc oxide powder (^{nat}ZnO) via the ^{64}Zn(n,p)^{64}Cu reaction in Tehran Research Reactor (TRR) and the activity values were compared with each other. The theoretical activity of ^{64}Cu also was calculated with MCNPX-2.6 and the cross sections of this reaction were calculated by using TALYS-1.8, EMPIRE-3.2.2 and ALICE/ASH nuclear codes and were compared with experimental values. Transmission Electronic Microscopy (TEM), Scanning Electronic Microscopy (SEM) and X-Ray Diffraction (XRD) analysis were used for samples characterizations. From these results, it's concluded that ^{64}Cu activity value with nanoscale target was achieved more than the bulk state target and had a good adaptation with the MCNPX result.

1. Introduction

Radioactivity in spite of its dangerous nature, it finds application in medicine both in diagnosis and therapy. Each application, however, requires a special kind of radionuclide (Qaim et al., 2017). ^{64}Cu is a beneficial and favorable radionuclide among other copper radionuclides, it emits low energy positrons with the endpoint energy of 653 keV and average energy of 278 keV (Qaim et al., 2017). This radionuclide also has medium energy beta particle ($E_{mean\ \beta^-}$ = 190 keV) (Johnsen et al., 2015), gamma radiation (E_γ = 1345.77 keV (0.473%), 511 keV (34.79%)) and an appropriate half-life ($t_{1/2}$ = 12.7 h) (Bokhari et al., 2010) allows a combination of PET scan with radiotherapy (Qaim et al., 2017).

^{64}Cu can be produced via ^{64}Ni(p,n)^{64}Cu reaction as a suitable reaction for reaching high production yields by cyclotron up to about 18 MeV, whereas the disadvantage of this reaction is the high costs of enriched ^{64}Ni (Thieme et al., 2012; Le et al., 2009). ^{64}Cu can also be produced in a nuclear reactor with ^{64}Zn(n,p)^{64}Cu and ^{nat}Zn(n,p)^{64}Cu reactions (Johnsen et al., 2015; Bokhari et al., 2010; Cohen et al., 2016; Uddin et al., 2014, 2013; Hassanein et al., 2006; Spahn et al., 2004; Van Elteren et al., 1999; Mushtaq et al., 1990; Fritze, 1964; Hetherington et al., 1986). The advantages of these reactions are low production costs, reasonable cross section and convenience separation ^{64}Cu from target with no radionuclide impurities except ^{67}Cu with minor activity. ^{67}Cu has same element with ^{64}Cu and needs complex chemical separation methods to remove (Cohen et al., 2016). The cross section of ^{67}Cu production is about 1.07 ± 0.04 mb (Bokhari et al., 2010) and during irradiation of ^{nat}Zn target with ^{67}Zn(n,p)^{67}Cu reaction can be produced with minor activity (Cohen et al., 2016). In 2010, the cross section of ^{64}Zn(n,p)^{64}Cu reaction has been reported by Bokhari et al. about 31 ± 2.3 mb. The production yield of ^{64}Cu has been reported by irradiating of 1 g ^{nat}Zn in Pakistan Research Reactor-1 and with a separation method based on column chromatography technique (Bokhari et al., 2010). On the other hand, small amounts of ^{64}Cu has been

* Corresponding author.
E-mail address: sadeghi.m@iums.ac.ir (M. Sadeghi).

https://doi.org/10.1016/j.apradiso.2018.03.007
Received 10 January 2018; Received in revised form 17 February 2018; Accepted 9 March 2018
Available online 12 March 2018
0969-8043/

produced using the nuclear reactions of $^{64}Zn(d,2p)^{64}Cu$ and $^{68}Zn(p,\alpha n)^{64}Cu$ (Qaim and Spahn, 2017).

Application of nanoparticles in radionuclide production has aimed to develop diagnosis and therapeutic techniques (Bakht et al., 2011). The most important characteristic of radioactive nanoparticles is its ability to have several radioactive atoms in one single nanoparticle. (Aboudzadeh et al., 2015). In the past decade, the activity of particles in bulk and nano forms has been studied. Soltani et al. investigated the activity of ^{141}Ce. They showed that the activity of ^{141}Ce produced with nano Ceria is less than the activity of simple Ceria particles (Soltani et al., 2015). Other researches in this case can be mentioned that ^{198}Au, $^{141}Pr_2O_3$ and $^{137\,m}Ce$ radionuclides productions (Hosseini et al., 2016; Bakht et al., 2012, 2011).

In present work, the production of ^{64}Cu have been experimented through irradiating natural zinc oxide and natural zinc oxide nanoparticles targets based on $^{nat}Zn(n,p)^{64}Cu$ reaction and the activity at the end of bombardment (EOB) of ^{64}Cu have been compared from bulk and nano scales targets. Transmission Electronic Microscopy (TEM), Scanning Electronic Microscopy (SEM) and X-Ray Diffraction (XRD) analysis have been done to distinguish targets characterization. The theoretical activity value have been calculated with MCNPX-2.6 code and the cross sections data also have been calculated with TALYS-1.8, EMPIRE-3.2.2 and ALICE/ASH theoretical codes for all of the opened channels. The obtained consequences have been compared to the theoretical and available experimental data.

2. Material and methods

2.1. Material

Zinc oxide nanoparticles powder has been purchased from US Research Nanomaterials, Inc. (Houston, USA). The physical properties and chemical composition of ZnONPs were reported by US Research Nanomaterials, Inc. are presented in Table 1. Zinc oxide powder also has been provided with 99% purity. The isotopic composition of zinc element with natural abundance was ^{64}Zn (48.6%), ^{66}Zn (27.9%), ^{67}Zn (4.1%), ^{68}Zn (18.8%) and ^{70}Zn (0.6%).

2.2. Cross section calculations

Recently, many experimental methods have been developed to evaluate the cross sections of various reactions (Kakavand et al., 2010). Therefore, the nuclear reaction cross sections data are significant for several technical applications such as medical radionuclide production, accelerator-driven systems, fission, fusion, dosimetry, radiation therapy and etc. (Koning et al., 2013). In this study cross sections of $^{64}Zn(n,p)^{64}Cu$ reaction has been estimated with TALYS-1.8, ALICE/ASH and EMPIRE-3.2.2 nuclear model code systems (Koning et al., 2013; Broeders et al., 2006; Herman et al., 2013). The calculated data has been compared with available experimental cross sections data and theoretical data such as ENDF/B-VII.1 library, which is latest theoretical nuclear data for use in nuclear science and technology applications (Chadwick et al., 2011).

2.2.1. TALYS-1.8

One of the powerful software which can be used for cross section calculations and to generate nuclear data is TALYS code. TALYS-1.8 is the latest update version that include neutrons, photons, protons, deuterons, tritons, ^3He, and α-particles as a projectile on target nuclei. The projectile energy range can be selected between 1 keV and 200 MeV. This program can calculate compound, direct and pre-equilibrium nuclear reactions which contains nuclear model parameters and nuclear level densities. In the latest version low energy resonance cross sections, more models for gamma-ray strength functions and for alpha optical potential are developed and also, the range of elements as a nuclide in the input file is extended up to Z = 12 (Koning et al., 2013; Rostampour et al., 2016). In this code, the OMP parameters were used to acquire a good fitted results with the experimental data.

2.2.2. EMPIRE-3.2.2

EMPIRE-3.2.2 is a modular system of nuclear reaction codes which is released in 1980. This code is composed of a number of linked FORTRAN codes and experimental data library. The incident projectiles can be chosen photons, nucleons and light or heavy ions. The energy range can be considered in neutron-induced reactions is above the resonance region to several hundred MeV for heavy-ion reactions (Rostampour et al., 2016; Azizakram et al., 2016). The quantum mechanical model and classical model to explain pre-equilibrium reactions is contained in this code (Herman et al., 2013). In this code, the level density parameters were used.

2.2.3. ALICE/ASH

ALICE/ASH is one of the nuclear code which is an update version of Blann code with intermediate energy projectiles up to 300 MeV (Sadeghi et al., 2011). ALICE/ASH can be used for cross section calculations, scattering investigations and residual nuclear yields of secondary particles in nuclear reactions (Yiğit and Kara, 2017; Sadeghi and Enferadi, 2011). The geometry dependent on hybrid model (GDH) is used for the description of the pre-equilibrium particle emission and the equilibrium calculations were made using Weisskopf–Ewing (W–E) model (Sadeghi et al., 2010; Şahan et al., 2016). In this code, the Hybrid model was used for pre-equilibrium reaction.

2.3. Experimental method

Irradiation process has been carried out using ^{nat}ZnO and $^{nat}ZnONPs$ powder as targets which were filled in quartz tubes and then cold welded in aluminum can separately. The weight of each sample was 1 ± 0.0001 g. The targets were irradiated with fast neutrons via 1.4×10^{13} n/cm^2 s flux in Tehran Research Reactor (TRR) with power of 4 MW for 30 min to produce ^{64}Cu by the $^{64}Zn(n,p)^{64}Cu$ reaction. The irradiated targets were dissolved in 10 ml 10 M HCl and were diluted for measurement. After 60 h cooling time the gamma-ray spectra and radionuclide purity of samples without any chemical separation were determined with a p-type high pure germanium detector (HPGe) coupled with a multichannel analyzer (MCA) (Silena International, Rome, Italy). In the gamma-ray spectra, the number of counts and detector efficiency for the selected peak were used to calculate the activity of radionuclide, using the following equation (Yeltepe and Yücel, 2018):

Table 1
Physical properties and chemical composition of $^{nat}ZnONPs$.

Purity (%)	Average particle size (nm)	Specific surface area ($m^2\ g^{-1}$)	True density ($g\ cm^{-3}$)	Crystal phase	Morphology	Color
Physical properties of $^{nat}ZnONPs$						
99+	10–30	20–60	5.606	Single	Nearly spherical	Milky white
Chemical composition of $^{nat}ZnONPs$						
ZnO	Cu	Mn	Cd	Pb		
≥ 99%	≤ 3 ppm	≤ 5 ppm	≤ 9 ppm	≤ 9 ppm		

$$A_{EOB} = \frac{N_c}{t\varepsilon_c I_\gamma}. \quad e^{\lambda t_{cool}} \tag{1}$$

where A_{EOB} is the activity at the end of bombardment (Bq = disintegration per second), N_c is the number of counts (net peak area) (dimensionless), t is the detector live time (s), ε_c is the counting efficiency for the detector at the corresponding gamma-ray energy (dimensionless), I_γ is the emission probability for the corresponding gamma-ray (dimensionless), λ is the decay constant of corresponding radionuclide and t_{cool} is the cool-down time (s).

2.4. Separation of ^{64}Cu from neutron irradiated zinc

In 2010, the separation method based on anion exchange column has been reported by Bokhari et al. In this method the 1 g Zn powder, after cool-time to decay short lived radionuclides, were dissolved in 10 ml 10 m HCl. The bath dried up by heating and then two times, distilled water has been added to remove excess of acid. After that, the residue was dissolved in 15 ml 12 m acetic acid and passed the anion exchange column (AG 1-X8 Cl- form, 100–200 mesh, 10 g), at rate of 1 ml/min which was washed with 25 ml 12 m acetic acid to wash the ^{64}Cu and zinc stays was eluted with 110 ml 0.1 M HCl. The yield of ^{64}Cu after chemical separation was 90% (Bokhari et al., 2010).

2.5. Simulation method by the MCNPX code

The theoretical activity calculations after irradiation of the samples can be calculated as following equation (IAEA, 2003):

$$A_{EOB} = N\sigma\Phi\left(1-e^{-\lambda t_{irr}}\right) \tag{2}$$

Where A_{EOB} is the activity of end of bombardment (EOB) (Bq = disintegration per second), N is the number of atoms of the target element, λ is the decay constant of ^{64}Cu (s^{-1}), t_{irr} is the irradiation time (s), σ is the fast neutron capture cross section (cm^2) and Φ is the fast neutron flux ($n\,cm^{-2}\,s^{-1}$). One of the empirical relations to describe the fission neutron spectrum was introduced by Cranberg et al. (normalized to 1 from 0 MeV to infinity) as follows (Cranberg et al., 1956; Omar et al., 2011):

$$P(E) = 0.453\times e^{-1.036E} \times \sinh\sqrt{2.29E}\,\frac{1}{MeV} \tag{3}$$

The fast neutron spectrum in the target has been calculated by the MCNPX-2.6 nuclear code so the reactor core of TRR has been simulated with the precise details of the core. The TRR is the only facility for reactor-based production of radionuclides which is pool-type, light water as cooling and shielding, 28 sets of standard fuel element (SFE) and 14 packages of graphite box with maximum power of 5 MW (in this work 4 MW). The TRR simulated as shown in Fig. 1, was considered 9 × 6 array with fuel plates, graphite boxes as efficient reflectors for reaching to the much more neutron economy around the core and irradiation boxes (Hosseini et al., 2017; Zandi et al., 2017). For this purpose, 1 g of ^{nat}ZnO was simulated in D6 site as a target in to the quartz tube with dimensions 41.6 mm long, 8 mm outside diameter, 6.4 mm inner diameter as target in the irradiation box. The fast neutron spectrum is achieved by fitting the curve according to the following equation (taken from the Cranberg et al. spectrum) to the values achieved from the F4/E4 card:

$$\varphi(E)(=n_0 vP(E)) \cong ce^{-aE}\sinh\sqrt{bE}\,\frac{n}{cm^2 s\ MeV} \tag{4}$$

where n_0 and v- are the total neutron density and the neutron velocity respectively. Constant coefficients of a, b and c is defined by the results of MCNPX code. Therefore, by the neutron energy distribution φ(E) at the ^{nat}ZnO-target site in the fast regions and the cross sections achieved from TALYS-1.8 code, the below integration have been solved:

$$\varphi\sigma = \int_{\text{Fast enegy region}} \varphi(E)\sigma(E)dE \tag{5}$$

By using the Eq. (2), the activity of ^{64}Cu can be calculated and the results have been compared with the experimental values as a benchmark data.

2.6. XRD, TEM and SEM analysis

XRD (STOE STADI, MP, Germany) has been used in determining the crystallite size and chemical formula of targets. TEM and SEM images of zinc oxide nanoparticles have been performed from Iranian Nanomaterials Pioneers Company, NANOSANY (Mashhad, Iran) before irradiation with fast neutrons to characterize their size and shape of them. After irradiation SEM images of zinc oxide nanoparticles also has been performed with Digital SEM (EM 3200 KYKY) to characterize the size and morphology changes of ZnONPs.

3. Results and discussion

3.1. Cross section of ^{64}Zn(n,p)^{64}Cu reaction

Commercially available ^{nat}ZnONPs and ^{nat}ZnO have been used to produce ^{64}Cu with ^{64}Zn(n,p)^{64}Cu reaction. The cross section calculations for ^{64}Zn(n,p)^{64}Cu reaction has been determined with the nuclear codes as mentioned before at the energy range up to 20 MeV in comparison with EXFOR data and theoretical cross sections data as shown in Fig. 2. There are good agreements between TALYS 1.8 code compared to experimental data (Santry and Butler, 1972; Huang et al., 1999; Lapenas et al., 1975; Mannhart and Schmidt, 2007) and theoretical cross sections database at the whole energy range. The EMIPRE-

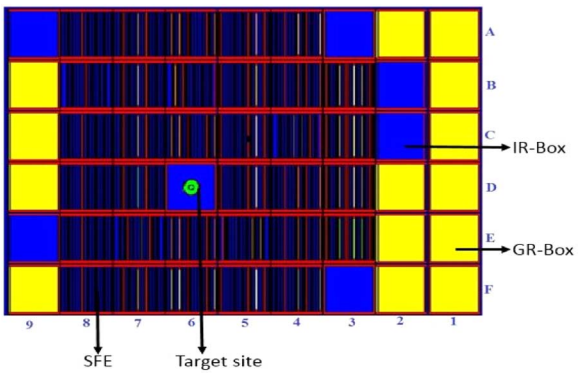

Fig. 1. Simulation of the core geometry and location of the ^{nat}ZnO-target by the MCNPX Visual Editor.

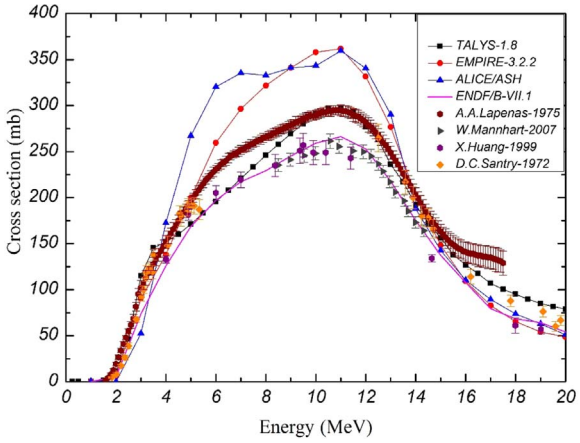

Fig. 2. Cross section of ^{64}Zn(n,p)^{64}Cu reaction calculated by ALICE/ASH, EMPIRE-3.2.2 and TALYS-1.8 codes along with experimental and theoretical values.

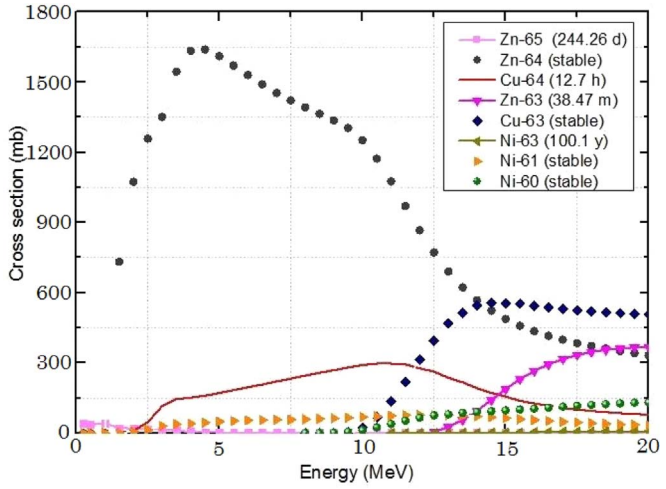

Fig. 3. Cross section of ^{64}Zn(n,p)^{64}Cu reaction and the residual radionuclides calculated by TALYS-1.8 code.

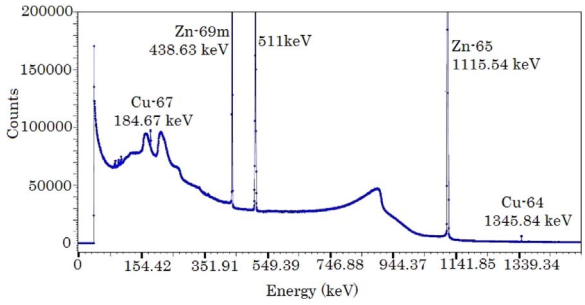

Fig. 4. Gamma spectra of ZnO by the gamma HPGe-MCA system.

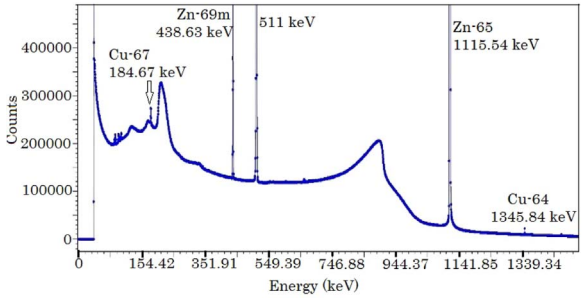

Fig. 5. Gamma spectra of ZnONPs by the gamma HPGe-MCA system.

Table 2
The activity of ^{64}Cu samples at EOB with neutron flux of 1.4×10^{13} n cm^{-1} s^{-1} for 30 min.

Activity MBq/ (1 g of ^{nat}ZnO and ^{nat}ZnONPs)				
Theoretical (MCNPX and TALYS code)	Relative difference (with Exp. 1)	Experimental Exp. 1	Exp. 2	Relative difference (with Exp. 1)
		^{64}Cu (^{nat}ZnO target)	^{64}Cu (^{nat}ZnO-NPs target)	
50.73	0.0148	46.29	55.96	0.1069

Relative difference = (Cal. – Exp.)/Cal.

3.2.2 calculation and ALICE/ASH grossly overestimated the cross sections and there are significant discrepancies in data set between 5 and 15 MeV approximately. Fig. 3 shows the cross sections of ^{64}Cu production with fast neutrons and the produced radionuclide impurities

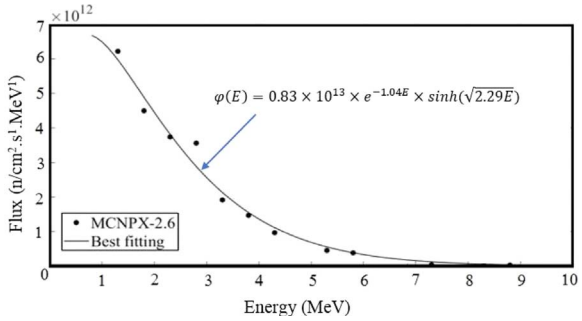

Fig. 6. Fast neutron energy spectrum at the target site by the MCNPX code and the best fitted function.

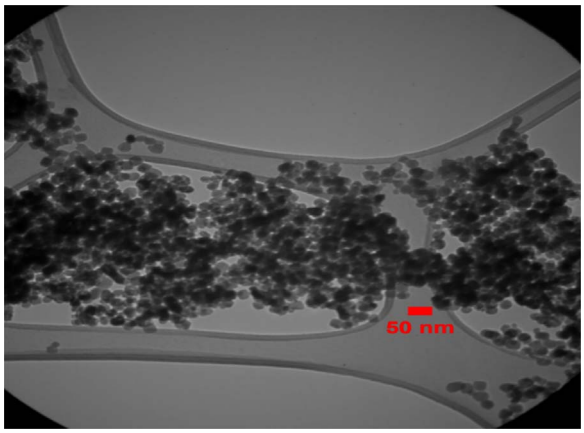

Fig. 7. Transmission Electron Micrograph (TEM) of zinc oxide nanoparticles from Iranian Nanomaterials Pioneers Company, NANOSANY.

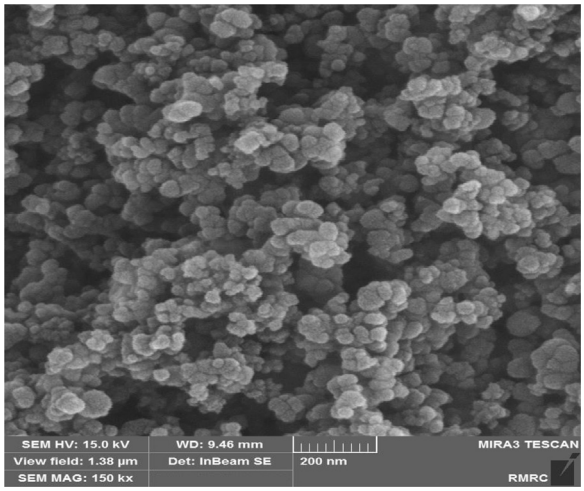

Fig. 8. Scanning Electron Microscope (SEM) of zinc oxide nanoparticles from Iranian Nanomaterials Pioneers Company (NANOSANY), before irradiation with fast neutrons.

which have been estimated with TALYS-1.8 code. ^{65}Zn ($T_{1/2}$ = 244.26 d), ^{63}Zn ($T_{1/2}$ = 38.47 m) and ^{63}Ni ($T_{1/2}$ = 100.1 y) radionuclides as impurities and the ^{63}Cu, ^{60}Ni and ^{61}Ni as stable nuclides were produced.

3.2. Experimental results

In this study. The irradiated ^{nat}ZnO and ^{nat}ZnONPs have been kept for about 60 h and after that the gamma spectra have been taken with HPGe detector (see Figs. 4 and 5). 1345.84 keV photopeak is ^{64}Cu characteristic and the 511 keV photopeak is related to its annihilation

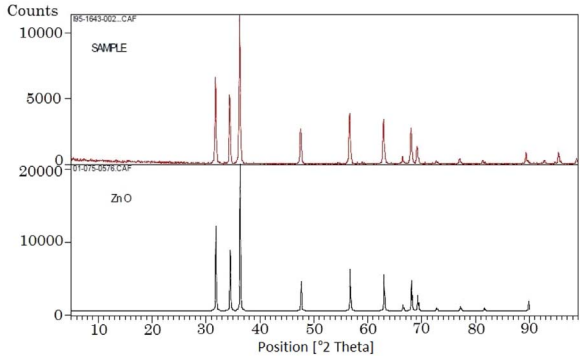

Fig. 9. XRD patterns of ZnO from STOE STADI, MP, Germany.

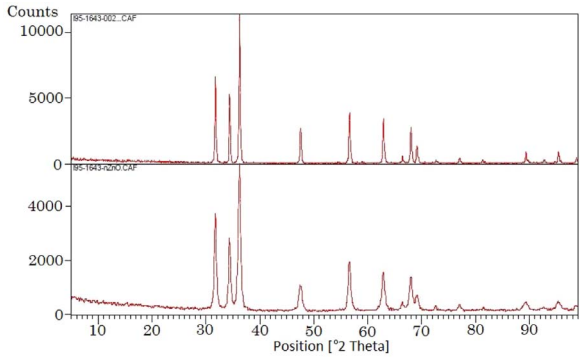

Fig. 10. XRD patterns of ZnONPs from STOE STADI, MP, Germany.

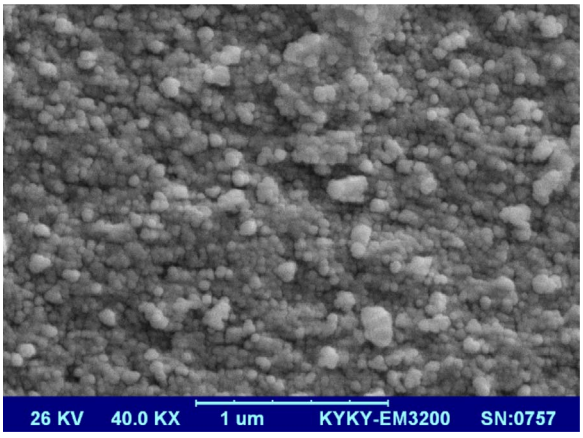

Fig. 11. Scanning Electron Microscope (SEM) of zinc oxide nanoparticles from Digital Scanning Electron Microscope EM 3200 KYKY, after irradiation with fast neutrons.

for β^+ emission and the counting of 1345.84 keV photopeak by HPGe reached to 117 and 371 CPS after 46.48 min and 126 min for ^{64}Cu and its nanoscale, respectively and the activity value at EOB of bulk state (49.98 MBq) and nanoscale (55.96 MBq) of mentioned radionuclide have been estimated by Eq. (1) with relative difference of 0.1069. Incremental activity value of the ^{64}Cu with nano scale target were observed (see Table 2). On the 10–30 nm scale, many of the atoms were located on the surface which is not observed in the bulk or individual atoms so the properties depend on the size of the structure like cross section value and production yield were changed.

As can be seen in Fig. 4, ^{67}Cu ($T_{1/2}$ = 61.83 h), ^{69m}Zn ($T_{1/2}$ = 13.76 h), and ^{65}Zn ($T_{1/2}$ = 244.26 d), have been produced as impurities via the ^{67}Zn(n,p)^{67}Cu, ^{68}Zn(n,γ) ^{69m}Zn and ^{64}Zn(n,γ) ^{65}Zn reactions and Fig. 5 also shows the same impurities which are related to nano scale target.

3.3. Theoretical results

The fast neutron distribution at the target site was calculated by the MCNPX with the best fitted is shown in Fig. 6 and the spectrum does behave like the fitted function which is taken from the Cranberg et al. spectrum. The normalize function for the MCNPX values was extracted as follows:

$$P(E) = 0.83\times10^{13} \times e^{-1.04E} \times \sinh\sqrt{2.29E}\,\frac{1}{MeV} \quad (6)$$

The theoretical activity at EOB of ^{64}Cu by using Eq. (2) have been calculated and with the experiment are listed in Table 2.

3.4. Characterization of ZnO and ZnONPs

TEM and SEM images and size distribution graph of ZnONPs before irradiation process with an average size of 20 nm spherical shapes are shown in Figs. 7 and 8 respectively. Figs. 9 and 10 are related to XRD of zinc oxide particles and zinc oxide nanoparticles, respectively. The average size of ZnONPs with XRD analysis has been estimated about 27 nm. XRD analysis has been displayed in the ZnO chemical formula of each samples. The SEM images of nanoparticle after irradiation as shown in Fig. 11, which clearly indicated that the shape of ZnONPs are spherical with no significant changes in their size.

4. Conclusions

This work, was developed for comparison activity at EOB of ^{64}Cu radionuclide via zinc oxide and zinc oxide nanoparticles separately from the ^{nat}Zn(n,p)^{64}Cu reaction which shows the increment activity when nano scale targets were used. The good agreement was obtained between the experimental results and calculated results by using MCNPX. The SEM, TEM and XRD analyses of target before and after irradiation were a demonstration of great achievement. Cross sections data were done with TALYS-1.8, ALICE/ASH and EMPIRE-3.2.2 codes and the EXFOR data and theoretical results displayed good agreements with TALLYS-1.8 code but on the other hand two other nuclear codes data showed exaggerated results.

References

Aboudzadeh, M.R., Moassesi, M.E., Amiri, M., Shams, H., Alirezapour, B., Sadeghi, M., Keyvani, M., 2015. Preparation and characterization of chitosan-capped radioactive gold nanoparticles: neutron irradiation impact on structural properties. J. Iran. Chem. Soc. 13, 339–345.

Azizakram, H., Sadeghi, M., Ashtari, P., Zolfagharpour, F., 2016. An overview of ^{124}I production at a medical cyclotron by ALICE/ASH, EMPIRE-3.2.2 and TALYS-1.6 codes. Appl. Radiat. Isot. 112, 147–155.

Bakht, M.K., Sadeghi, M., Ahmadi, S.J., Sadjadi, S.S., Tenreiro, C., 2012. Preparation of radioactive praseodymium oxide as a multifunctional agent in nuclear medicine: expanding the horizons of cancer therapy using nanosized neodymium oxide. Nucl. Med. Commun. 34, 5–12.

Bakht, M.K., Sadeghi, M., Tenreiro, C., 2011. A novel technique for simultaneous diagnosis and radioprotection by radioactive cerium oxide nanoparticles: study of cyclotron production of ^{137m}Ce. J. Radio. Nucl. Chem. 292, 53–59.

Bokhari, T.H., Mushtaq, A., Khan, I.U., 2010. Production of low and high specific activity ^{64}Cu in a reactor. J. Radioanal. Nucl. Chem. 284, 265–271.

Broeders, C.H.M., Konobeyev, A.Y., Korovin, Y.A., Lunes, V.P., Blann, M., 2006. ALICE/ASH Pre-compound and evaporation model code system for calculation of excitation functions, energy and angular distributions of emitted particles in nuclear reaction at intermediate energies. FZK-7183. ⟨http://bibliothek.fzk.de/zb/berichte/FZKA7183.pdf⟩.

Chadwick, M.B., Herman, M., Oblozˇinsky, P., Dunn, M.E., Danon, Y., Kahler, A.C., Young, P.G., 2011. ENDF/B-VII.1 Nuclear data for science and technology: cross sections, covariances, fission product yields and decay data. Nucl. Data Sheets 112, 2887–2996.

Cohen, I.M., Segovia, M.S., Bedregal, P.S., Mendoza, P.A., Aguirre, A.R., Montoya, E.H., 2016. A novel method for determination of copper in zinc destined to ^{64}Cu production in a nuclear reactor. J. Radioanal. Nucl. Chem. 309, 23–26.

Cranberg, L., Frye, G., Nereson, N., Rosen, L., 1956. Fission neutron spectrum of U-235. Phys. Rev. 103, 662.

Fritze, K., 1964. The preparation of high specific activity copper 64. Radiochim. Acta 3, 166–167.

Hassanein, M.A., El-Said, H., El-Amir, M.A., 2006. Separation of carrier-free ^{64,67}Cu radionuclides from irradiated zinc targets using 6-tungstocerate (IV) gel matrix. J. Radioanal. Nucl. Chem. 269, 75–80.

Herman, M., Capote, R., Sin, M., Trkov, A., Carlson, B.V., Obloz˘insky, P.,…, Zerkin, V., 2013. EMPIRE-3.2 Malta modular system for nuclear reaction calculations and nuclear data evaluation. ⟨http://www.iaea.org/inis/collection/NCLCollectionstore/_Public/44/117/44117920.pdf⟩.

Hetherington, E., Sorby, P.J., Camakaris, J., 1986. The preparation of high specific activity copper-64 for medical diagnosis. Appl. Radiat. Isot. 37, 1242–1243.

Hosseini, S.F., Sadeghi, M., Aboudzadeh, M.R., Mohseni, M., 2016. Production and modeling of radioactive gold nanoparticles in Tehran research reactor. Appl. Radiat. Isot. 118, 361–365.

Hosseini, S.F., Sadeghi, M., Aboudzadeh, M.R., 2017. Theoretical assessment and targeted modeling of TiO_2 in reactor towards the scandium radioisotopes estimation. Appl. Radiat. Isot. 127, 116–121.

Huang, X., Weixiang, Yu, Han, X., Zhao, W., Hanlin, L., Chen, J., Zhang, G., 1999. The effect of low-energy neutrons on activation cross-section measurement. Nucl. Sci. Eng. 131, 267–274.

IAEA, 2003. Vienna. Manual for reactor produced radioisotopes. IAEA-TECDOC-1340, 63.

Johnsen, A.M., Heidrich, B.J., Durrant, Ch.B., Bascom, A.J., Unlu, K., 2015. Reactor production of ^{64}Cu and ^{67}Cu using enriched zinc target material. J. Radioanal. Nucl. Chem. 305, 61–71.

Kakavand, T., Sadeghi, M., Alipoor, Z., 2010. Nuclear model calculation on charged particle induced reactions to produce ^{85}Sr for diagnostic and endotherapy. Kerntechnik 75, 263–270.

Koning, A.J., Hilaire, S., Goriely, S., 2013. TALYS-1.8: A Nuclear Reaction Program" User Manual. NRG, Netherlands. ⟨http://www.talys.eu/download-talys⟩.

Lapenas, A.A., Bondars, Kh.J., Vejnbergs, J.K., 1975. Evaluated data for neutron dosimetry reactions. Lapenas Neutron Spect. Meas. by Activ. Riga.

Le, V.S., Howse, J., Zaw, M., Pellegrini, P., Katsifis, A., Greguric, I., Weiner, R., 2009. Alternative method for ^{64}Cu radioisotope production. Appl. Radiat. Isot. 67, 1324–1331.

Mannhart, W., Schmidt, D., 2007. Measurement of neutron activation cross sections in the energy range from 8 MeV to 15 MeV. Physikalisch-Technische Bundesanstalt, Braunschweig (Germany) Neutronen physic.

Mushtaq, A., Karim, H.M.A., Khan, M.A., 1990. Production of no-carrier-added ^{64}Cu and ^{67}Cu in a reactor. J. Radioanal. Nucl. Chem. 141, 261–269.

Omar, H., Khattab, K., Ghazi, N., 2011. Neutron energy spectra calculation in the low power research reactor. Indian. J. Pure Appl. Phys. 49, 723–730.

Qaim, S.M., Spahn, I., 2017. Development of novel radionuclides for medical applications. J. Label. Compd. Radiopharm. http://dx.doi.org/10.1002/jlcr.3578.

Rostampour, M., Aboudzadeh, M.R., Sadeghi, M., Hamidi, S., 2016. Theoretical assessment of production routes for ^{63}Zn by cyclotron. J. Radioanal. Nucl. Chem. 309, 677–684.

Sadeghi, M., Enferadi, M., 2011. Nuclear model calculations on the production of ^{119}Sb via various nuclear reactions. Ann. Nucl. Energy 38, 825–834.

Sadeghi, M., Enferadi, M., Nadi, H., 2010. Study of the cyclotron production of ^{172}Lu: an excellent radiotracer. J. Radioanal. Nucl. Chem. 286, 259–263.

Sadeghi, M., Zandi, N., Bakhtiari, M., 2011. Nuclear model calculation for cyclotron production of ^{61}Cu as a PET imaging. J. Radioanal. Nucl. Chem. 292, 777–783.

Şahan, M., Tel, E., Şahan, H., Gevher, U., Kara, A., 2016. Cross section calculations of (n, 2n) and (n, p) nuclear reactions on germanium isotopes at 14–15 MeV. J. Fusion. Energ. 35, 730–742.

Santry, D., Butler, J., 1972. Excitation curves for the reactions of fast neutrons with zinc. Can. J. Phys. 50, 2536–2548.

Soltani, F., Samani, A.B., Sadeghi, M., Shirvani, A.S., Yavari, K., 2015. Production of cerium-141 using ceria and nanoceria powder: a potential radioisotope for simultaneous therapeutic and diagnostic applications. J. Radioanal. Nucl. Chem. 303, 385–391.

Spahn, I., Coenen, H.H., Qaim, S.M., 2004. Enhanced production possibility of the therapeutic radionuclides ^{64}Cu, ^{67}Cu and ^{89}Sr via (n, p) reactions induced by fast spectral neutrons. Radiochim. Acta 92, 183–186.

Thieme, S., Walther, M., Pietzsch, H.J., Henniger, J., Preusche, S., Mading, P., Steinbach, J., 2012. Module-assisted preparation of ^{64}Cu with high specific activity. Appl. Radiat. Isot. 70, 602–608.

Uddin, M.S., Sudár, S., Hossain, S.M., Khan, R., Zulquarnain, M.A., Qaim, S.M., 2013. Fast neutron spectrum unfolding of a TRIGA Mark II reactor and measurement of spectrum-averaged cross sections: integral tests of differential cross sections of neutron threshold reactions. Radiochim. Acta 101, 613–620.

Uddin, M.S., Zaman, M.R., Hossain, S.M., Qaim, S.M., 2014. Radiochemical measurement of neutron -spectrum averaged cross sections for the formation of ^{64}Cu and ^{67}Cu via the (n,p) reaction at a TRIGA Mark-II reactor: feasibility of simultaneous production of the theragnostic pair ^{64}Cu/^{67}Cu. Radiochim. Acta 102, 473–480.

Van Elteren, J.T., Kroon, K.J., Woroniecka, U.D., De Goeij, J.J.M., 1999. Voltammetry detection of copper in high specific activity ^{64}Cu. Appl. Radiat. Isot. 51, 15–19.

Yeltepe, E., Yücel, H., 2018. Standardization of ^{142}Pr activity concentration. Appl. Radiat. Isot. 134, 263–268.

Yiğit, M., Kara, A., 2017. Model-based predictions for nuclear excitation functions of neutron-induced reactions on $^{64,66-68}$Zn targets. Nucl. Eng. Technol. 49, 996–1005.

Zandi, N., Afarideh, H., Aboudzadeh, M.R., Rajabifar, S., 2017. Study on a new design of Tehran Research Reactor for radionuclide production based on fast neutrons using MCNPX code. Appl. Radiat. Isot. 132, 67–71.